Journal of Colloid and Interface Science 393 (2013) 161–173

Contents lists available at SciVerse ScienceDirect

Journal of Colloid and Interface Science

www.elsevier.com/locate/jcis

Structure, thermodynamics and dynamics of the isotropic phase of spherical non-ionic surfactant micelles

Kévin Tse-Ve-Koon [a,b], Nicolas Tremblay [a], Doru Constantin [c], Éric Freyssingeas [a,*]

[a] Université de Lyon, Laboratoire de Physique, École Normale Supérieure de Lyon, CNRS-UMR 5672, 46 allée d'Italie, 69364 Lyon, France
[b] Université de Lyon, CREATIS CNRS-UMR 5220, INSERM-U1044, INSA-Lyon, Université Lyon 1, Lyon, France
[c] Université Paris-Sud, Laboratoire de Physique des Solides, CNRS-UMR 8502, 91405 Orsay, France

ARTICLE INFO

Article history:
Received 13 July 2012
Accepted 19 October 2012
Available online 8 November 2012

Keywords:
Micellar solution
Non-ionic surfactant
Small-Angle Neutron Scattering
Quasi Elastic Light Scattering
High Frequency Rheology

ABSTRACT

We investigate a non-ionic surfactant ($C_{12}E_8$)/water binary mixture, over a wide range of concentrations and temperatures (*i.e.* 1–35 wt.% of $C_{12}E_8$ and 10–60 °C in temperature) by means of different experimental techniques: Small-Angle Neutron Scattering (SANS), Quasi Elastic Light Scattering (QELS) and High Frequency Rheology. The aims of this work are to provide information on structure, thermodynamics and dynamics of the isotropic phase of such a micellar system and, by combining these different types of information, to obtain a comprehensive image of the behaviour of this phase. Our results demonstrate that structural, thermodynamic and dynamic properties of these solutions are fully monitored by the temperature-induced changes in the ethylene–glycol chain hydration. They confirm that $C_{12}E_8$ micelles are spherical and do not grow in the investigated range of concentrations and temperatures. They demonstrate that the interaction potential between $C_{12}E_8$ micelles is more complicated than what was previously described, with an additional repulsive interaction. They allow us to put forward explanations for the Isotropic–Ordered phase transition as well as for the temperature behaviour of the viscosity of $C_{12}E_8$ micellar solutions. Our investigation provides new and valuable information on the dynamics of these mixtures that reflect the complexity of the interaction potential between the $C_{12}E_8$ micelles. It shows that concentrated solutions exhibit a viscoelastic behaviour that can be described by a simple Maxwell model.

1. Introduction

Non-ionic surfactants do not have electrical charge, which makes them very interesting for many applications in a wide range of different areas. For example, because they do not bear charge, these surfactants are resistant to water hardness deactivation and thus they are excellent grease removers that are widely used in laundry products, household cleaners and hand dishwashing liquids. On a fundamental point of view, these surfactants provide very interesting model systems to investigate as they can form dispersions of aggregates (that can be spheres, cylinders or bilayers) with no long-range repulsion.

Among these surfactants, one finds the octa-ethylene–glycol mono *n*-dodecylether (also named: $C_{12}E_8$; $C_{12}H_{25}$–$(OCH_2CH_2)_8$–OH), which is a non-ionic surfactant routinely used in many biotechnical applications, for example, in the process of extraction/reconstitution of membrane proteins and for making liposomes [1–11]. In aqueous solution, this surfactant displays interesting and puzzling features. Like other surfactants in the C_iE_j family (consisting of a hydrophobic chain with *i* carbons and a hydrophilic head containing *j* ethylene–glycol groups), the temperature–concentration phase diagram of $C_{12}E_8/H_2O$ mixture shows a wide and rich variety of thermodynamic liquid crystalline phases (cubic, hexagonal, lamellar), critical points and binodal curves, as well as an isotropic phase over a large range of both temperatures and concentrations. Its phase diagram is, however, noticeably different from those of $C_{12}E_j/H_2O$ mixtures with $j \leqslant 7$, although these surfactants are not much different chemically [12–23]. Particularly, $C_{12}E_8/H_2O$ system exhibits a cubic phase (I1) and do not display lamellar phase ($L\alpha$) over a wide range of temperatures and surfactant concentrations. These features are also observed for $C_{12}E_j/H_2O$ mixtures with $j \geqslant 9$. The general consensus is that these differences are due to the hydrophilic head of $C_{12}E_8$ molecule that is larger than for $C_{12}E_j$ with $j \leqslant 7$, which increases the spontaneous curvature of the surfactant monolayer [21–23].

Although this surfactant is widely used, surprisingly, there are relatively few studies with a "physical" point of view on the isotropic phase of $C_{12}E_8/H_2O$ mixture [5,8,23–37] and therefore several interrogations still remain. The first investigations on this mixture were carried out more than 25 years ago [24–26]. Using SANS experiments, Zulauf et al. [25] studied the structure of isotropic phases

* Corresponding author.
E-mail address: eric.freyssingeas@ens-lyon.fr (É. Freyssingeas).

0021-9797/$ - see front matter © 2012 Elsevier Inc. All rights reserved.
http://dx.doi.org/10.1016/j.jcis.2012.10.039

of different non-ionic surfactants, including $C_{12}E_8$, over a wide range of concentrations (typically: 2.5–35% in mass) and temperatures (30–60 °C). Since this pioneering work, other investigations have been conducted on this problem as, for example, that of Imai et al. [34]. These later studies, however, mostly focused on the part of the phase diagram that is in the vicinity of the Isotropic–Ordered phase transition, hence on rather concentrated solutions (around 35 wt.%) and low temperatures (below 20 °C). The conclusions drawn from these different works appear somehow contradictory. This is particularly true regarding the interaction potential between $C_{12}E_8$ micelles. There seems to be a consensus that interaction potential between $C_{12}E_8$ micelles is the sum of two contributions: a hard sphere potential and an attractive potential of Yukawa type. However, on the one hand, Zulauf et al. [25] claim that the range of hard sphere part is the equal to the micelle radius and the attractive part is of short range (smaller than 5 Å) and increases as temperature rises and $C_{12}E_8$ concentration decreases. At low temperature and high concentration, its strength is very weak while it is rather strong (larger than $10k_BT$) at high temperature and low concentration. On the other hand, Imai et al. (using the SAXS technique) [34] find different features; the range of the hard sphere potential is smaller than the micelle radius, while the attractive potential has strength of the order of k_BT with a long range (20–30 Å) and is observable for high concentrations (typically within 30–40 wt.%) and low temperature (below 20 °C).

According to Zulauf et al. [25], $C_{12}E_8$ micelles remain spherical with temperature and this assertion seems to be corroborated by other works [29–32] that used different techniques. This is, indeed, rather surprising since it is commonly accepted that C_iE_j surfactant micelles grow and become worm-like as the temperature goes above $(T_c - 30)$ °C, approximately, where T_c is the critical consolute temperature. In the case of the $C_{12}E_8$/water system, the consolute temperature is of about 75 °C and therefore one would expect micellar growth above 45 °C, a feature that is not observed in Refs. [25,29–32]. Nevertheless, this assertion is questioned by some other works, such as Hedin et al. using NMR [33], which allegedly observed the growth of $C_{12}E_8$ micelles with increasing T. Thus, do $C_{12}E_8$ micelles grow with temperature? If not, then the reason provided to explain the behaviour of the viscosity of $C_{12}E_8$ micellar solutions with T [35] must be ruled out and a new explanation must be found.

Another intriguing property of this system is that it exhibits a phase transition between the isotropic phase and an ordered phase of spheres (of hcp symmetry) upon decreasing T for $C_{12}E_8$ mass concentrations included between 31 and 38 wt.%. At first sight, this seems impossible. For such temperatures, $C_{12}E_8$ micelles are spherical, $C_{12}E_8$ density is given to be of the order of one and there is no long-range interaction between micelles. Therefore, the existence of such a phase transition is difficult to understand. Even considering the hydration of the polar headgroup, an explanation does not seem that obvious. As this transition occurs upon temperature decreasing, it suggests that the head group hydration as well as the aggregation number is monitored by temperature. How? Do they depend on concentration? This has never been investigated precisely.

Furthermore, one may also notice that the dynamical properties of the isotropic phase of $C_{12}E_8/H_2O$ mixture, especially in the "high" concentration part of the phase diagram (*i.e.* for $C_{12}E_8$ mass fraction > 15%) were not much investigated. A few studies were carried out by means of Quasi Elastic Light Scattering experiments [34,38–40], but they mainly focused on dilute mixtures.

For all these reasons, the aim of this study is to obtain a comprehensive image of the isotropic phase of the $C_{12}E_8/H_2O$ mixture over a wide range of concentrations and temperatures. For such a purpose, we used different experimental techniques: structural techniques such as Small-Angle Neutron Scattering (SANS), which provides direct insight into the thermodynamics of the mixture as well as spectroscopy techniques such as Quasi Elastic Light Scattering: (QELS) and rheology, which probe the dynamic behaviour of the system. Combining these different types of information allows us to show that the interaction potential between $C_{12}E_8$ micelles is more complicated than what was previously described; to confirm that $C_{12}E_8$ micelles do not grow and remain spherical with temperature (at least up to 60 °C); to explain the Isotropic–Ordered phase transition as well as the temperature behaviour of the viscosity; to provide new and valuable information on the dynamics of these systems. Moreover, we believe that our results have a much more general interest. They could also prove useful for other C_iE_j–water mixtures (particularly for of C_iE_j molecules having a polar headgroup volume much bigger than that of their hydrophobic chain; *e.g.* $C_{12}E_j$, with $j > 9$), pluronic–water mixtures, as well as dispersions of spherical colloids covered with PEO or PEG chains.

2. Experimental section

2.1. Materials

The surfactant $C_{12}E_8$ was purchased from Nikko Chemicals Ltd. and used without further purification. We used ultrapure water ($\rho = 18 \pm 0.1$ MΩ cm) from an in-house ELGA system to prepare the $C_{12}E_8/H_2O$ samples used for Quasi Elastic Light Scattering as well as rheology measurements. For Small-Angle Neutron Scattering experiments, $C_{12}E_8$ was mixed with D_2O from Aldrich (see Supporting Material: Part A.1). The samples were prepared by weighing both components into vials. The obtained mixtures were carefully homogenised by repeated heating, stirring, and centrifuging and then allowed to equilibrate at room temperature over a few days (in the dark since $C_{12}E_8$ may undergo a chemical degradation with light). We finally obtain homogenous, transparent solutions, which are in the isotropic state at room temperature.

For SANS experiments, we prepared 5 $C_{12}E_8/D_2O$ samples, with mass fractions of $C_{12}E_8$ (w_S) equal to: 5, 10, 18, 25, and 35 wt.%, respectively. For QELS and rheology experiments, 7 different $C_{12}E_8/H_2O$ samples were prepared having w_S equal to 1, 5, 10, 18, 25, 30, and 35 wt.%, respectively.

2.2. Methods

2.1.1. SANS experiments (Supporting Material: Part A.2)

The five samples were all investigated at five different temperatures: 10 °C, 20 °C, 30 °C, 40 °C and 50 °C, respectively. (These experiments were carried out on the D11 diffractometer at the high flux reactor of the Institut Laue-Langevin (ILL) in Grenoble.) SANS profiles were recorded in the wave vectors range: 3.93×10^{-3}–0.247 Å^{-1}; that is,: 3.93×10^{7}–2.47×10^{9} m^{-1}. Following ILL standard procedures, raw data were treated to yield normalised scattering intensities $I(q)$ (cm^{-1} units) [41,42].

2.1.2. QELS experiments (Supporting Material: Part A.2)

All the $C_{12}E_8/H_2O$ samples were investigated in the temperature range 10 °C–50 °C, where they are in the isotropic phase, except for the sample with $w_S = 35$ wt.% that undergoes an Isotropic–Ordered phase transition at about 15 °C. This latter sample was investigated in the temperature range 16 °C–50 °C. For the five D_2O samples used for SANS experiments, we investigated dynamic properties at 20 °C, 40 °C and 50 °C, respectively. For each investigated sample and at all temperatures, we recorded the time autocorrelation functions of the scattered intensity, namely: $\langle I(0)I(t)\rangle$ every 10° between 20° and 150° (*i.e.* q varying in the range: 3.74×10^{6}–3.31×10^{7} m^{-1}). For each scattering angle, we took five autocorrelation functions. No polariser was placed in front of the detector to

analyse the polarisation state of the scattered light. However, before carrying out the experiments, we checked that the depolarised scattering signal was negligible. Hence, we considered that we only measured polarised scattering.

2.1.3. High frequency rheology experiments (Supporting Material: Part A.2)

High frequency rheology measurements were performed in a piezorheometer, and the principle of which was described in Ref. [43]. This setup allows us to measure the complex viscosity $\tilde{\eta}$ for frequencies ranging from 1 rad/s to 6.28×10^4 rad/s from which we can deduce both the storage (G') and loss (G'') shear moduli. We have already performed a preliminary investigation of the $C_{12}E_8/D_2O$ mixtures [44]. Here, we extend this study to the $C_{12}E_8/H_2O$ mixtures over a wider concentration range, carrying out the experiments on the seven samples that are investigated in light scattering. For sample with $w_S = 1$ wt.%, measurements were performed for seven temperatures: 5, 10, 20, 30, 40, 50 and 60 °C, respectively. For samples with $w_S = 5$, 10 and 18 wt.%, experiments were performed at 13 different temperatures: every 5 °C, from 4 °C to 64 °C. For samples with $w_S = 30$ and 25 wt.%, we investigated the same temperatures as those probed for samples with the same mass concentration in the $C_{12}E_8/D_2O$ mixtures [44]. For that with $w_S = 35$ wt.%, rheological properties were investigated at 16 °C and every 4 °C between 18 °C and 66 °C. Finally, for the five SANS samples, we studied their rheological properties at 20 °C, 40 °C and 50 °C, respectively.

3. Results

3.1. SANS experiments

Except for the lowest concentration investigated ($w_S = 5$ wt.%) at 50 °C, the scattering profiles always exhibit a well-defined bump, more or less pronounced depending on w_S and T (Fig. 1). One observes that for a given temperature, the location of the top of the scattering bump q^* moves towards the smallest values of q as concentration decreases (Fig. 1a). For the small q values, the scattering intensity decreases as concentration increases. At large q values, the scattering intensity increases with concentration. Nevertheless, it appears that the scattering intensity on the right hand-side of the scattering bumps decays the same way for all concentrations. For a given concentration, one observes that the position at which the maximum of the scattering bump is located moves towards the smallest values of q as T increases (Fig. 1b) and the scattering bump gets broader. At low q, the scattering intensity increases with T. At large q, we notice that all scattering profiles fall on the same curve for all temperatures. From these observations, two conclusions can be drawn.

(i) The scattering at large q indicates that likely the shape and size of the surfactant aggregates do not change much with w_S and T.
(ii) The scattering bump suggests the existence of a spatial correlation; a "short-range" structure characterised by a local order that evolves with w_S and T. Decreasing the concentration appears having the same effect as increasing temperature; both variations lead to a broadening of the scattering bump and a displacement of its top towards small q, indicating a loss of correlation.

3.2. QELS experiments

For all samples with $w_S \geqslant 10$ wt.%, measured autocorrelation functions always appear to be bimodal for all wave vectors over the entire range of investigated temperatures and therefore they are fitted to the following test function: $\langle I(0)I(t)\rangle = (A_1 e^{-\Omega_1 t} + A_2 e^{-\Omega_2 t})^2 + B$, where Ω_1 and Ω_2 are the fast and slow frequencies, respectively (Supporting Material: Part B.1, Fig. S.1a). Ω_1 is always at least two orders of magnitude larger than Ω_2. This bimodal relaxation of the autocorrelation functions of the scattered light intensity was already observed in $C_{12}E_8$–water mixtures by Brown et al. [38]. As in our investigation, they observe the slow relaxation mode only for mass concentrations w_S larger than 10 wt.%. For samples with $w_S = 1$ and 5 wt.%, the measured autocorrelation functions are always monomodal; only the fast mode remains (Supporting Material: Part B.1, Fig. S.1b). For all experimental conditions, the five measured values of Ω_1 (as well as those of Ω_2) are very close to each other, and in the following, we show their average values.

3.2.1. Fast relaxation

For all samples at all investigated temperatures, the measured values of Ω_1 scale with the scattering wave vector q like q^2: $\Omega_1 = Dq^2$ (Fig. 2a), corresponding to a diffusive process. The values of the diffusion coefficient D are plotted as a function of temperature for the different $C_{12}E_8$ concentrations in Fig. 2b. Except for sample with $w_S = 1$ wt.%, for which the diffusion coefficient seems to linearly increase with T, the temperature evolution of D is non-monotonic and depends on w_S. Since there is no depolarised scattering signal, we assume that micelles are spherical. Fig. 2c displays the ratio $D(T)/D_0(T)$ as a function of T, where $D_0(T) = k_BT/6\pi\eta_S(T)r_1(T)$, $\eta_S(T)$ being the solvent viscosity at the temperature T and $r_1(T)$ the micelle radius returned by SANS experiments at this temperature (see Supporting Material: Fig. S.5a). For sample with $w_S = 1$ wt.%, this quantity is always close to 1. Hence, we conclude that for this sample, D is simply the free micelle diffusion coefficient; $D = k_BT/6\pi\eta_S r_h$, where r_h is the micelle hydrodynamic radius. The measured values of r_h ($r_h = k_BT/6\pi\eta_S D_{Measured}$) slightly increase with T, from 31 ± 2 Å to 34 ± 2 Å as T goes from 10 °C to 50 °C, in very good agreement with the micelle radii measured by SANS experiments. For samples with $w_S \geqslant 5$ wt.%, the ratio $D(T)/D_0(T)$ decreases exponentially with T with a decay constant that is all the smaller as the concentration is high (inset Fig. 2c). For samples with $w_S \geqslant 5$ wt.%, the ratio $D(T)/D_0(T)$ decreases exponentially with T, the decay constant (T_D) dropping with increasing surfactant concentration (Fig. 2c). There, QELS experiments probe the relaxation of concentration fluctuations. In that case, the measured diffusion coefficient D corresponds to the collective diffusion coefficient D_c.

3.2.2. Slow relaxation

The contribution of the slow mode to the autocorrelation function (*i.e.* its magnitude) decreases continuously with increasing q; it is barely observable above $\theta = 120°$. We notice that $A_2(q)$ drops as w_S decreases as well as with increasing T. We do not observe any relationship between Ω_1 and Ω_2, suggesting that these two relaxations have different physical origins. It is quite difficult to obtain accurate measurements of Ω_2; at low q, this frequency is very slow, often at the limit of the correlator range (furthermore, at these small scattering angles, the signal may be polluted by the presence of small dust particles in the sample); at large q, its amplitude becomes very low, making the estimation of Ω_2 rather difficult. Therefore, the measurement uncertainty is rather large although the values of Ω_2 for a given scattering angle are well reproducible from one measurement to another. We can, however, reasonably describe Ω_2 as a function of q by: $\Omega_2 = D_2q^2$ (Fig. 2d). In that case, this slow relaxation would be due to diffusive processes, with diffusion coefficients D_2 ranging from about 10^{-13}–10^{-14} m^2s^{-1}, thus 3 orders of magnitude below the diffusion coefficient of the fast mode D_c. Nevertheless, this mode could be super-diffusive; the

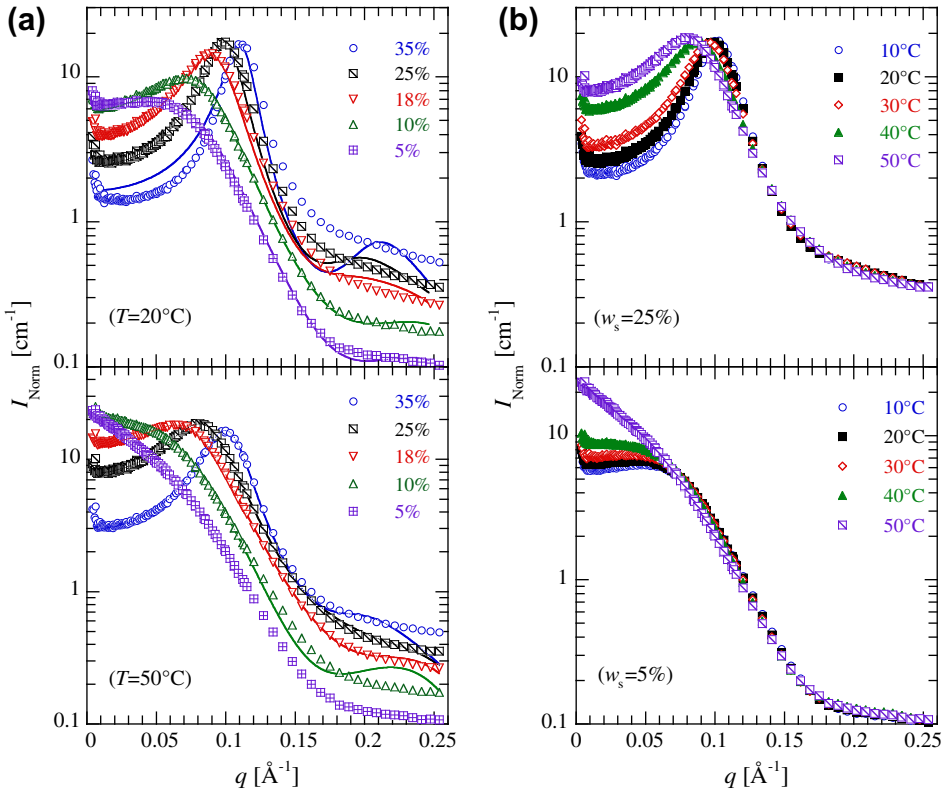

Fig. 1. (a) Small-Angle Neutron Scattering profiles obtained at T = 20 °C and 50 °C, respectively, on the different investigated samples. Lines are the fits to "Zulauf's Model" (see Supporting Material; Part C.1, Eq. S.17) (b) SANS profiles obtained on the samples with a mass concentration of $C_{12}E_8$ equal to 25 wt.% and 5 wt.%, respectively, for T = 10 °C, 20 °C, 30 °C, 40 °C and 50 °C.

best fits of Ω_2 are, indeed, given by the function: Cq^{α} where C is a constant and α a free parameter that is always larger than 2; it is found between 2.2 and 2.4 (Fig. 2d).

3.3. High frequency rheology experiments

For all investigated concentrations and temperatures, the real part of the complex viscosity, η', is constant as a function of frequency over almost four decades (Supporting Material: Part B.2, Figs. S.2 and S.3). The zero-shear viscosity of the samples η is given by the position of this plateau. In Fig. 3a, the reduced viscosity: $\eta^* = \eta_{sample}(T)/\eta_S(T)$, where η_S is the solvent viscosity, is displayed as a function of T. For all concentrations, we observe the same features. First η^* decreases as T increases, passes through a minimum, then increases with T. For the most concentrated samples, this increase reaches a maximum and then η^* decreases again at higher temperature. The positions of these minima and maxima move with w_S; both shifting towards lower temperatures as w_s increases. This behaviour was also observed by D'Arrigo et al. [35]. In this reference, the authors claim that this behaviour is first due to the growth of the $C_{12}E_8$ micelles with T (transformation of spherical micelles into worm-like micelles), which gives rise to the increase in viscosity and then to their connection, leading to the decrease of viscosity. However, in light of our results and the investigations carried out by Zulauf et al. [25], Jonstromer et al. [31] and Danino et al. [32], showing that the $C_{12}E_8$ micelles remains spherical in the concentration and temperature ranges we investigated, this explanation seems rather unlikely. Furthermore, in the case of micelle growth, one should observe a much stronger increase in η^* with T as well as the appearance of a "low frequency" viscoelastic behaviour. This is the case for example for $C_{12}E_6/H_2O$ solutions [44] or $C_{12}E_5/H_2O$ mixtures ([45] and Supporting Material: Part C.3, Figs. S.14 and S.15). Therefore, it is clear that the scenario proposed in Ref. [35] must be ruled out.

It is also observed that concentrated solutions (typically $w_S \geqslant 30$ wt.%) exhibit viscoelastic behaviour in the frequency range accessible to our rheometer (Supporting Material: Part B.2, Fig. S.4). This behaviour has never been observed before. Likely because with a "classical" rheometer that cannot probe frequencies larger than 100 s^{-1}, it is difficult to observe the viscoelastic properties of these mixtures. The values of G'' increase linearly with ω over almost the entire frequency range (this corresponds to the plateau of η'). The values of G' are only detectable above about 300 s^{-1} (where they exceed the sensitivity of the apparatus, which is of the order of 1 Pa) and they scale with the frequency like ω^2. The frequency evolutions of G' and G'' never cross within the frequency range, and we can investigate, nevertheless, their behaviour with ω is compatible with a single Maxwell process. Thus, we fit the spectra using the Maxwell model [46]:

$$G^*(\omega) = G'(\omega) + iG''(\omega) = \frac{G_\infty(\omega\tau)^2}{1-(\omega\tau)^2} + i\frac{G_\infty\omega\tau}{1-(\omega\tau)^2} \quad (1)$$

where G_∞ is the high frequency shear modulus and τ the Maxwell relaxation time, with: $G_\infty = \eta/\tau$ (η being the zero-shear viscosity). For a given w_S, as T increases, the frequency at which G' becomes detectable increases and finally no viscoelastic behaviour can be observed any longer at high temperature. Values of G_∞ and τ returned by the fits to the Maxwell model can be considered as valuable only below 46 °C. Fig. 3b and c shows the temperature evolutions of τ and G_∞, respectively, for both samples. The obtained values of τ are of the order of magnitude for both samples (a few 10^{-6} s) and decrease as T increases. The values of G_∞ are larger for w_S = 35 wt.%

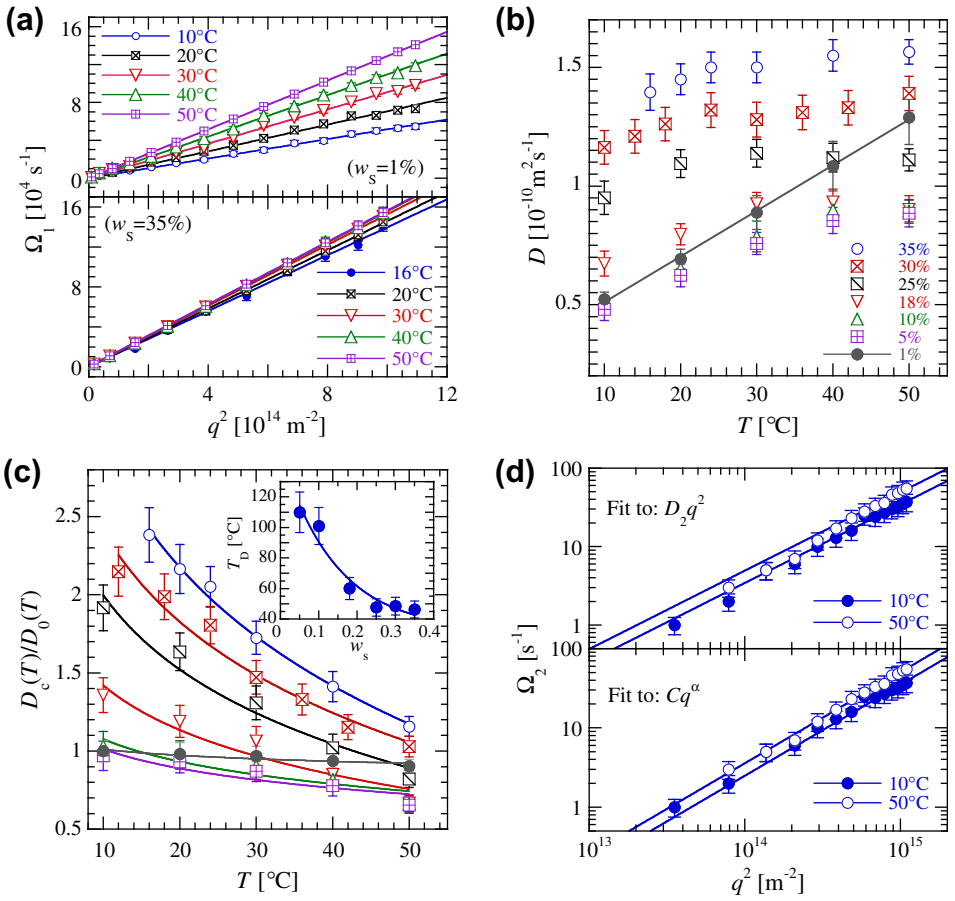

Fig. 2. (a) Average values of Ω_1 as a function of q^2 for samples with w_S = 1 and 35 wt.%, respectively, for different temperatures. (b) Measured values of D as a function of T for all investigated samples. (c) $D(T)/D_0(T)$ as a function of T, where $D_0(T) = k_BT/6\pi\eta_S(T)r_1(T)$. Lines are the fits of $D(T)/D_0(T)$ to $a(w_S)\exp(-T/T_D(w_s))$. Inset: values of T_D as a function of w_S. (d) Average values of Ω_2 as a function of q^2 for sample with w_S = 25 wt.% at 10 °C and 50 °C, respectively. Solid lines correspond to the curve fits (here $\alpha = 2.4 \pm 0.1$ for both temperatures).

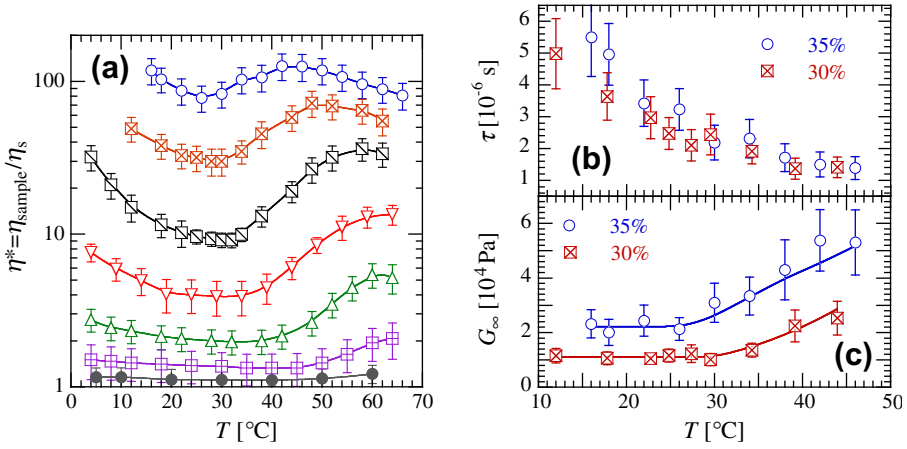

Fig. 3. (a) Reduced viscosity: $\eta^* = \eta_{sample}(T)/\eta_S(T)$, as a function of T (semi-log scale) for all investigated samples (same set of markers as in Fig. 2b). Solid lines are guide for eyes. (b) Measured values of the Maxwell relaxation time τ as a function of T for samples with w_S = 30 and 35 wt.%, respectively. (c) Evolution of G_∞ as a function of T for these two samples. Solid lines are guide for eyes.

than for 30 wt.%; nevertheless, their temperature evolution is the same: G_∞ seems to be constant as T increases up to about 25–30 °C, then it grows with T.

Here, it should be noted that raw measurements obtained on $C_{12}E_8/D_2O$ mixtures are different from those obtained for $C_{12}E_8/H_2O$ samples. However, it is observed that the values of the "normalised" quantities (*i.e.* $D(T)/D_0(T)$ and η^*) as well as their evolution with concentration and temperature are very similar. Hence, we believe that $C_{12}E_8/D_2O$ and $C_{12}E_8/H_2O$ mixtures are very similar systems and we can use information obtained through SANS experiments on $C_{12}E_8/D_2O$ samples to interpret experiments carried out on $C_{12}E_8/H_2O$ solutions.

4. Discussion

4.1. Shape, structure and interaction

SANS profiles are the product of two distinct terms: the form factor $P(q)$, accounting for the shape and size of the surfactant aggregates and the structure factor $S(q)$ that is the Fourier transform of the aggregate pair correlation function. $I(q) = n_m P(q) S(q)$, where n_m is the number of scattering centres per unit volume, here the density of surfactant aggregates: $n_m = N_m/V = \phi_m/V_m$ (V being the scattering volume, N_m the number of aggregates within the volume V, ϕ_m the volume fraction of the aggregates and V_m the volume of a single aggregate).

First of all, the SANS data were analysed using the same model as Zulauf et al. [25] and Imai et al. [34] (results of the analysis are shown and discussed in detail in Supporting Material, Part C.1). In this framework, $C_{12}E_8$ micelles interact through a potential $U_0(d)$ that is the superimposition of a hard sphere potential and an attractive potential of Yukawa type; the micelle form factor is that of a core–shell sphere. This model returns seven adjustable parameters: r_1 (micelle radius), r_2 (core radius), $\Delta\rho$ (difference in scattering length density between the $C_{12}E_8$ micelle shell and D_2O), $\Delta\rho_{CS}$ (difference in scattering length density between the core and shell of the $C_{12}E_8$ micelle), R (hard sphere radius), ϕ (volume fraction of hard spheres), U_0 (strength of the attractive part; $U_0 < 0$) and δ_0 (effective range of the attractive interaction). By setting R equal to r_1, as done by Zulauf et al. [25], we do not get agreement between SANS data and the model. On the other hand, letting both R and r_1 as free parameters, as done by Imai et al. [34], data can fit to the model. The obtained results confirm that $C_{12}E_8$ micelles are spheres within these concentrations and temperature ranges. This is in agreement with Ref. [25], QELS measurements (since we do not observed a slow, depolarised and independent q mode that would indicate the presence of rods), rheology measurements (since we do not observe viscoelastic behaviour at low concentration). The hard sphere radius R is always found to be slightly smaller than the micelle radius r_1, in agreement with Ref. [34]. For a given mass concentration, the effective volume fraction of hard sphere ϕ decreases with T; the number of micelles in solution is not only set by the $C_{12}E_8$ concentration, it is also a function of temperature (note that ϕ differs from the micelle volume fraction ϕ_m: $\phi = \phi_m V_{hs}/V_m = \phi_m R^3/r_1^3$, V_{hs} being the hard sphere volume.) On the other hand, from one scattering profile to another, the obtained fitting values for U_0 and δ_0 vary a lot, showing no kind of correlation between these parameters and $C_{12}E_8$ concentration or temperature. Therefore, we cannot conclude whether our experiments support Zulauf et al.'s [25] or Imai et al.'s [34] conclusions. We believe that this comes from a lack of description of the interaction potential. Since the hard sphere radius R is found smaller than the micelle radius r_1, $C_{12}E_8$ micelles (the hydrophilic heads of the surfactant molecules, *i.e.* the E_8 chains) can interpenetrate, which causes an additional repulsive interaction. SANS profiles, indeed, suggest the existence of this additional repulsive interaction between $C_{12}E_8$ micelles (for concentrated samples, scattering profiles are systematically always below the model at small q; Fig. 1a and Fig. S.8), as well as QELS and viscosity results (see next sections). So far, this additional repulsion has never been described.

One of the simplest models that can be used to describe the total interaction potential $U(d)$ between $C_{12}E_8$ micelles is to assume that the steric repulsion as well as the attraction can be described by repulsive and attractive potentials of Yukawa type. Hence, $U(d)$ writes as follows:

$$U(d) = \begin{cases} +\infty \quad \text{for} : d \leqslant 2R \\ U_{rep}\frac{2R}{d} exp\left(-\frac{(d-2R)}{\delta_{rep}}\right) + U_{att}\frac{2R}{d} exp\left(-\frac{(d-2R)}{\delta_{att}}\right) \quad \text{for} : d > 2R \end{cases} \tag{2}$$

where U_{rep} is the strength of the steric repulsive part ($U_{rep} > 0$); U_{att} is the strength of the attractive part ($U_{att} < 0$); δ_{rep} and δ_{att} express the measure of the effective range of the repulsive and attractive interaction, respectively. Assuming that steric repulsion and attraction are not long-range (*i.e.* random phase approximation [47]), an approximate analytical solution for the structure factor $S(q)$ is found [48]:

$$S_U(q) = \frac{1}{1 + \phi C_U(q)} \tag{3}$$

where $C_U(q) = C_{hs}(q) + C_{rep}(q) + C_{att}(q)$. $C_{hs}(q)$ accounts for the hard sphere contribution and is calculated using the Ornstein–Zernicke equation with the Percus–Yevick closure [49,50], while $C_{rep}(q)$ and $C_{att}(q)$ account for the steric and attractive interactions, respectively. Expressions of $C_{hs}(q)$ and $C_{att}(q)$ are given in: Supporting Material: Part C.1, Eqs. S.15 and S.16, respectively; $C_{rep}(q)$ is given by the following relations [34,48]:

$$\begin{aligned} C_{rep}(q) &= \frac{4\pi}{q}\int_{2R}^{\infty} sin(qr)(U_{rep}(r))rdr \\ &= \frac{6U_{rep}}{\pi}\left(\frac{\delta_{rep}}{2R}\right)\left(\frac{sin(2qR) + (q\delta_{rep})cos(2qR)}{2qR(1 + (q\delta_{rep})^2)}\right) \end{aligned} \tag{4}$$

The core–shell sphere form factor is written as:

$$\begin{aligned} P_{CS}(q) &= V_m^2 \Delta\rho^2 f(q) \quad \text{with} : f(q) \\ &= 9\left(\frac{j_1(qr_1)}{qr_1} + \frac{\Delta\rho_{CS}}{\Delta\rho}\left(\frac{r_2}{r_1}\right)^3 \frac{j_1(qr_2)}{qr_2}\right)^2 \end{aligned}$$

where $j_1(x) = (\sin(x) - x\cos(x))/x^2$ is the first-order spherical Bessel function. Hence, we may write $I(q)$ as:

$$\begin{aligned} I(q) &= n_m P_{CS}(q) S(q) = \frac{\phi_m}{V_m}\left(\frac{V_m^2 \Delta\rho^2 f(q)}{1 + \phi C_U(q)}\right) \\ &= \frac{\phi r_1^3}{R^3}\left(\frac{V_m \Delta\rho^2 f(q)}{1 + \phi(C_{hs}(q) + C_{rep}(q) + C_{att}(q))}\right) \end{aligned} \tag{5}$$

where ϕ is the volume fraction of hard spheres. Trying to fit $I(q)$ to this model allowing the nine parameters of Eq. (6) to be free is a non-sense that gives rise to incoherent results. Therefore, we divide $I(q)$ by $V_m \Delta\rho^2 f(q)$, to obtain a new quantity $\Sigma(q)$ that is proportional to $S(q)$:

$$\begin{aligned} \Sigma(q) &= \frac{\phi r_1^3}{R^3} S(q) \\ &= \frac{\phi(r_1^3/R^3)}{1 + \phi(C_{hs}(q, \phi, R) + C_{rep}(q, \phi, U_{rep}, \delta_{rep}) + C_{att}(q, \phi, U_{att}, \delta_{att}))} \end{aligned} \tag{6}$$

For each temperature, the function $V_m \Delta\rho^2 f(q)$ is calculated using the average values of r_1, r_2, $\Delta\rho$, and $\Delta\rho_{CS}$ obtained over the values returned by the fit of all $I(q)$ to "Zulauf's model". We arbitrarily decide to set r_1 equal to its measured value and δ_{rep} equal to 4 Å. (The typical range of the steric repulsion, δ_{rep}, is related to the difference between the hard sphere and micelle radii. Assuming that the values of R returned by the previous model are rather correct, this difference is of the order of 4 Å and does not seem to vary much. Setting the value of δ_{rep} equal to 3 or 5 Å instead of 4 Å does not change the results.) All the different $\Sigma(q)$ are fitted to Eq. (6) with five adjustable parameters: R, ϕ, U_{rep}, U_{att} and δ_{att}. Except for scattering profiles recorded on the most dilute samples at 50 °C, this model fits all the SANS data in the q range: 0.01–0.24 $Å^{-1}$ (for $q < 0.01$ $Å^{-1}$, the scattering signal is not reliable). However, this way of fitting $\Sigma(q)$ still does not allow us to observe coherent behaviours of U_{rep}, U_{att} and δ_{att} with concentration or temperature (most likely because these parameters influence each other).

Therefore, we set a constraint on δ_{att}. By forcing δ_{att} to be within the range 7–13 Å, all the $\Sigma(q)$ (still except that of 5% at 50 °C) can be fitted to Eq. (6) (Fig. 4), while trying to force δ_{att} to be smaller than 7 Å, or greater than 13 Å, does not all allow us to fit all the $\Sigma(q)$ to Eq. (6) with the same constraint. Under these conditions ($7\ \text{Å} \leqslant \delta_{att} \leqslant 13\ \text{Å}$), the agreement between the SANS data and this model is much better than with the "Zulauf's model", particularly at small angles, yielding a much better evaluation of $S(0)$ (Supporting Material: Part C.2; Figs. S.9–S.12). U_{rep} and U_{att} seem to be independent on concentration and increase with temperature, while no systematic variations of δ_{att} with w_S or T are observed (Supporting Material, Fig. S.9a). This latter suggests that the range of the attractive interaction should be of the order of 10 Å and is likely not very sensitive to concentration and temperature. Values of R and ϕ are little sensitive on how the fits are performed; their obtained values are always very close to those returned by the fitting of $\Sigma(q)$ to "Zulauf's model". Typically, the dispersion of the values is of the order of the uncertainty returned by the fits. The hard sphere radius is always found to be smaller than the micelle radius and of the order of 31 Å (Supporting Material, Fig. S.9b).

The obtained values of the volume fraction of hard spheres, ϕ, are displayed as a function of temperature in Fig. 5a. For a given mass concentration, ϕ decreases exponentially with T: $\phi(w_S, T) = w_S \exp(-(T - T_0)/T\phi)$, where T_0 is the temperature at which ϕ is equal to w_S, T_ϕ is the constant decay. Both T_0 and T_ϕ do not seem to depend on the $C_{12}E_8$ concentration. It is found: $T_0 = 46 \pm 3$ °C and $T_\phi = 73 \pm 5$ °C. Assuming an Arrhenius law, $\phi(w_S, T) = Aw_S \exp(E/k_BT)$ (T in Kelvin), with an activation energy $E = (1.73 \pm 0.15) \times 10^{-20}$ J, that is, $E = (4.2 \pm 0.4)k_BT$ (with $T = 300$ K), and $A = 0.0186 \pm 0.0005$. According to these results, for $w_S = 35$ wt.%, the effective volume fraction of hard spheres reaches the volume fraction at which solutions of hard spheres undergo a disordered–ordered phase transition: 0.494 [51,52], for a temperature of about 17–18 °C that corresponds to the Isotropic–Ordered transition temperature for this solution.

Because the amount of $C_{12}E_8$ molecules is set by the solution composition and the increase in r_1 is quite weak, the increase in the volume fraction of micelles as T decreases must involve an increase in the aggregation number, v_S, with T. This increase in v_S is the consequence of the dehydration of the E_8 chains with T (like for others C_iE_j surfactants [53–56]). $v_S = N_{C12E8}/N_m$ (N_{C12E8} being the number of surfactant molecules and N_m the number of micelles) thus $v_S = (4\pi R^3 N_A w_S \rho_{sol})/(3\phi M_{C12E8})$, where N_A is the Avogadro constant; M_{C12E8}, the $C_{12}E_8$ molar mass (538.8 g/mol); ρ_{sol}, the solution mass density (assumed to be equal to that of D_2O); ϕ, the hard sphere volume fraction; R, the hard sphere radius. v_S seems to be independent of w_S and increases with T as $1/\phi$, $v_S \propto \exp(T/T_\phi)$ (Fig. 5b), or $v_S \propto \exp(-E/k_BT)$, with $E = (1.73 \pm 0.15)10^{-20}$ J. It goes from about 85 at 10 °C to about 155 at 50 °C, yielding a decrease in the polar head area of $C_{12}E_8$ molecules ($\sigma = 4\pi r_1^2/v_S$) as T increases from about 160 Å^2 at 10 °C to 90 Å^2, approximately, at 50 °C. These values of v_S are in good agreement with the results obtained in Ref. [25,31,32] by means of Static Light Scattering experiments, NMR and time-resolved fluorescence quenching (v_S increases with T from about 90 at 20 °C to about 160 at 60 °C). Nevertheless, contrary to us, Ref. [25] finds that v_S very weakly depends on concentration.

From the values of v_S, the hydration number h_S can be estimated (the number of D_2O molecules bound to one E_8 chain): $h_S = (V_m - v_S V_{C12E8})/(v_S V_{D2O})$, V_{C12E8} is the volume of a $C_{12}E_8$ molecule: 797.5 Å^3 [25]. The average values of h_S obtained over the 5 concentrations are displayed in Fig. 5c. h_S decreases almost linearly as T increases the investigated temperature range; it goes from about 35 D_2O molecules per E_8 chain at 10 °C to about 10 at 50 °C (*i.e.* from about 4 D_2O molecules per ethylene oxide group to 1), in good agreement with the results of Refs. [25,31,32]. This temperature evolution suggests a complete dehydration of the hydrophilic chains for temperature in the range 72–78 °C, which corresponds to temperatures at which the micellar solutions undergo a phase separation between a $C_{12}E_8$ rich phase and water. Using these values of v_S or h_S, the volume of the hydrated polar headgroups can be calculated for each investigated temperature: $V_{headgroup} = (V_m/v_S) - V_{C12} = (V_{C12E8} - V_{C12}) + h_S V_{D2O}$, where V_{C12} is the volume of the alkyl chain, equal to about 327 Å^3 [5,25] ($V_{D2O} = 30$ Å^3). $V_{headgroup}$ goes from about 1460 Å^3 at 10 °C to 780 Å^3 approximately at 50 °C. Thus, the hydrated headgroup/alkyl chain volume ratio varies from about 4.5 at 10 °C to about 2.5 at 50 °C (Fig. 5d). As a consequence, the volume of the hydrated polar headgroup is thus always much larger than that of the alkyl chain, which leads to a cone shape for the hydrated $C_{12}E_8$ molecules. Thereby, the spherical shape of the $C_{12}E_8$ aggregates may be understood, at least qualitatively, by molecular shape arguments [57]. According to the $C_{12}E_8/H_2O$ phase diagram, it is very likely that this does not hold any longer at higher concentration (at about 40 wt.%, typically, close to L1–H1 transition) or at higher temperature (close to the critical consolute temperature; so above 70 °C). Note that taking into account the D_2O molecules bound to E_8 chains, the values of $\Delta\rho$ can be estimated for the different temperatures in a crude model; they are in good agreement with the experimental measurements (Supporting Material Fig. S.5b).

In Fig. 6a and b are displayed the fitting values of U_{rep} and U_{att} as a function of T, respectively, assuming $\delta_{rep} = 4$ Å and $7\ \text{Å} \leqslant \delta_{att} \leqslant 13$ Å. Both seem to be independent of w_S. U_{rep} augments with T; it can be noticed that U_{rep} increases with the density Γ of E_8

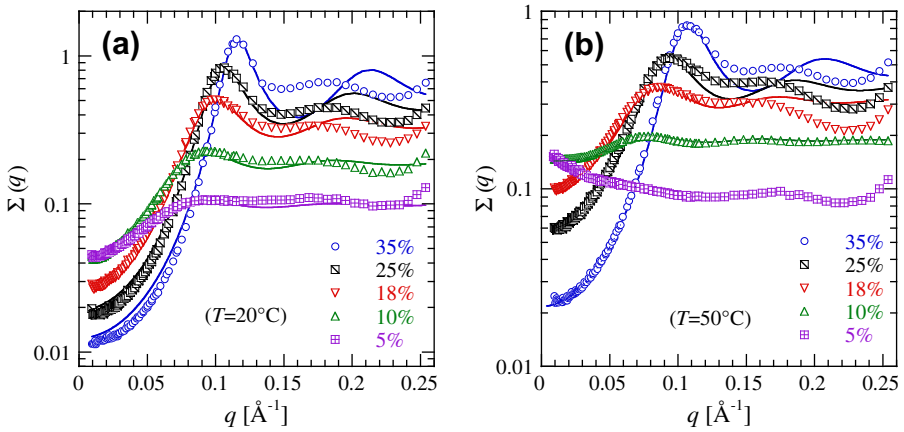

Fig. 4. $\Sigma(q)$ obtained at 20 °C (a) and 50 °C (b) for all investigated concentrations (for $q > 0.01$ Å^{-1}). Solid lines are the fits to Eq. (6), setting $\delta_{rep} = 4$ Å and $7\ \text{Å} \leqslant \delta_{att} \leqslant 13$ Å.

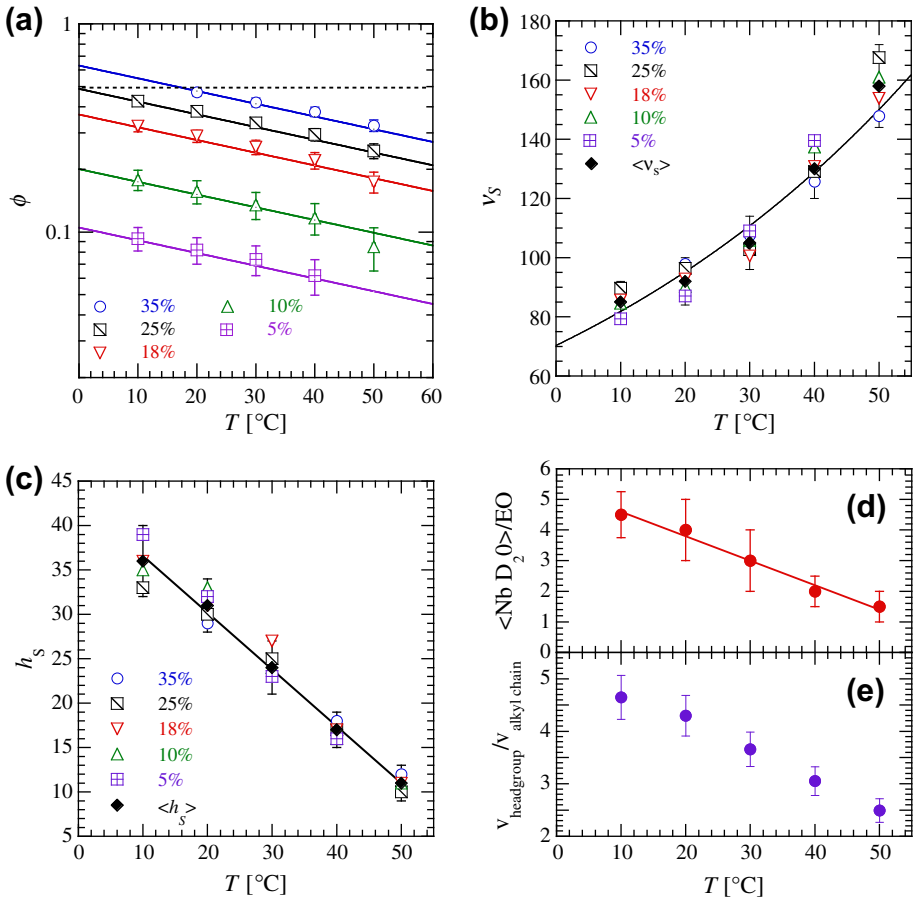

Fig. 5. (a) Measured volume fraction of hard sphere ϕ as a function of T for the different investigated samples; solid lines correspond to: $\phi(w_S, T) = w_S \exp(-(T - T_0)/T_\phi)$ (the horizontal dashed line indicates $\phi = 0.494$). (b) Values of the aggregation number v_S as a function of T. The black line corresponds to the fit of the average values $\langle v_S \rangle$ to $B \exp(T/T_\phi)$. (c) Measured values of the hydration number h_S as a function of T. (d) Measured average values of the number of D_2O per EO as a function of T. (e) Headgroup/alkyl chain volume ratio as a function of T.

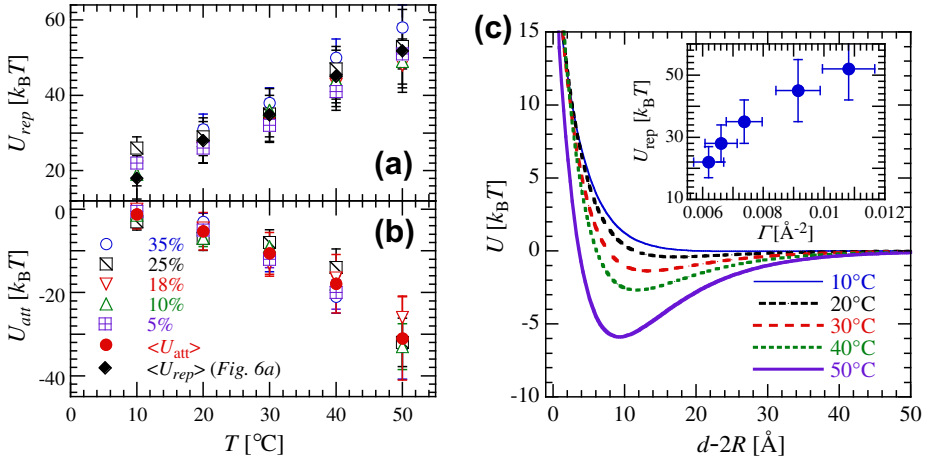

Fig. 6. (a) Values of U_{rep} as a function of T. (b) Values of U_{att}, as a function of T. (c) Estimation of the total interaction potential between micelles (in k_BT unit) as a function of the micelle–micelle separation (micelle–micelle distance minus hard sphere diameter), setting $\delta_{rep} = 4$ Å and $\delta_{att} = 10$ Å. Insert, U_{rep} as a function of the density of E_8 chains per micelle.

chains per micelle ($\Gamma = 1/\sigma = v_s/(4\pi r_1^2)$, inset Fig. 6c), which is consistent with steric interaction between polymers coated surfaces [58]. The strength of the attractive potential enhances as T increases. This is in agreement with Zulauf et al. [25]. Using the obtained average values of U_{rep}, and U_{att}, setting $\delta_{rep} = 4$ Å and $\delta_{att} = 10$ Å, we may estimate a total interaction potential U between $C_{12}E_8$ micelles as a function of their separation ($d - 2R$, the micelle–micelle distance minus the hard sphere diameter) for different temperatures (Fig. 6c). In this framework, U shows a strengthening of the effective attraction between micelles as T increases; with a

minimum that deepens while the effective range enhances. In this framework, the effective attraction between micelles is very weak at low temperatures and strengthens strongly above 30 °C. Because of the assumptions made, it is likely that this estimate of the interaction potential is rather crude. The obtained temperature evolution of U, however, is fully consistent with QELS and rheology results (Sections 4.2 and 4.3) as well as with the temperature–concentration phase diagram of $C_{12}E_8$–water mixtures.

4.2. Viscosity

In Fig. 7a, the reduced viscosity η^* is plotted as a function of the hard sphere volume fraction ϕ for all investigated samples (ϕ is calculated using the following relation: $\phi(w_S, T) = w_S \exp(-(T - T_0)/T_\phi)$ with $T_0 = 46$ °C and $T_\phi = 73$ °C). For all mass fractions, the same behaviour upon decreasing ϕ (so corresponding to an increase in T) is observed. The reduced viscosity decreases with ϕ down to a minimum and then increases up to a maximum to decrease again at lower volume fraction. One can notice that all the data points seem to be contained between two limits. A "low viscosity" limit that is given by: $(1 - \phi/\phi^*)^{-2}$, with $\phi^* = 0.54 \pm 0.02$ (the solid line on Fig. 7a). A "high viscosity" limit that can be described as a power series of : $\eta^* = 1 + 2.5\phi + k_2\phi^2 + k_3\phi^3$ with: $k_2 = 628 \pm 58$, $k_3 = 751 \pm 93$, (the dashed line on Fig. 7a). (Note that we imposed as the first term of this expansion the Einstein expression for dilute sphere suspensions: $\eta_{sample}/\eta_S \approx 1 + 2.5\phi$, because the interactions between micelles do not change the first coefficient, which is affected by the hydrodynamic interactions only and not by the sphere–sphere interaction, this latter only influencing terms in ϕ^n with $n \geqslant 2$, corresponding to binary, ternary, *etc.*, collisions.)

Fig. 7b displays the same set of data as in Fig. 7a, but now with all the measurements taken at a given temperature T gathered together (more precisely, measurements taken within a temperature range $T \pm 2$ °C). This shows the evolution of the "isothermal" reduced viscosity as a function of ϕ for different temperatures. In the temperature range 5–18 °C, all the values of η^* collapse on a master curve that seems to diverge at high volume fraction and fits to the "low viscosity" limit. This behaviour resembles the expected behaviour for pure hard sphere solutions: $\eta^* = (1 - \phi/\phi_{rcp})^{-2}$ where ϕ_{rcp} is the random close packing concentration; that is, $\phi_{rcp} = 0.63$ [59]. In this work the observed divergence of η^* at lower volume fraction is likely due to the additional steric interaction between micelles. Interaction between spheres distorts the particles trajectories more than if there were only hydrodynamic interactions between them, which enhances dissipation and thereby causes an increase in viscosity with respect to that of hard sphere solutions [60–62]. Thus, up to 18 °C the temperature-induced changes in the direct interaction between micelles do not modify much their hydrodynamic interactions (because these changes are weak). This is no longer true for higher temperatures. Between 18 °C and about 35 °C, the evolution of the reduced viscosity with ϕ can be fitted to: $\eta^* = (1 - \phi/\phi^*)^{-2}$, with a value of ϕ^* that depends on T, decreasing from 0.54 ± 0.02 at 18 °C to 0.46 ± 0.02 at 35 °C. The decrease in ϕ^* as temperature increases from 18 °C to 35 °C is most likely due to the augmentation of the attraction between micelles with T. Between 35 °C and about 58 °C, there is no obvious relationship between η^* and ϕ. Upon increasing the volume fraction, η^* crosses over from the "low viscosity" branch to the "high viscosity" branch. The effects of the increase in the micelle–micelle interaction on the hydrodynamic interactions become important and keep enhancing up to about 58 °C. Above 58 °C, η^* no longer depends on T, and all reduced viscosities fall on a master curve that is the "high viscosity" branch. This suggests that the effects of the direct interaction between micelles on the hydrodynamic interactions do not change with temperature any more.

These results suggest that the attraction between $C_{12}E_8$ micelles is weak at low temperatures, increases strongly when dehydration of the E_8 chains is important, *viz.* around 35 °C, and then, it stagnates once dehydration of the E_8 chains is almost complete. These inferences are, indeed, in total agreement and fully consistent with both SANS (see Fig. 6) and QELS observations (see next section). The values of k_2 and k_3 lead us to believe that the effect of the direct micelle–micelle interaction on the hydrodynamic interaction is strong. Nevertheless, for high temperatures, even at volume fractions larger 0.3, the solutions exhibit Newtonian flow at low shear rate, suggesting that both the strength and range of the direct interaction are always rather weak.

The temperature behaviour of the viscosity of $C_{12}E_8$ micellar solutions can be understood as follows. As temperature increases, there is a competition between two effects: on one side ϕ decreases, which causes a decrease in the reduced viscosity, and on the other side, at the same time, the attraction between micelles increases and this effect leads to an increase in the viscosity. For a given mass concentration, when the temperature is increased from very low temperatures, at first the decrease in the effective volume fraction of micelles dominates and the viscosity decreases with the volume fraction. Then, it is the increase in the attraction

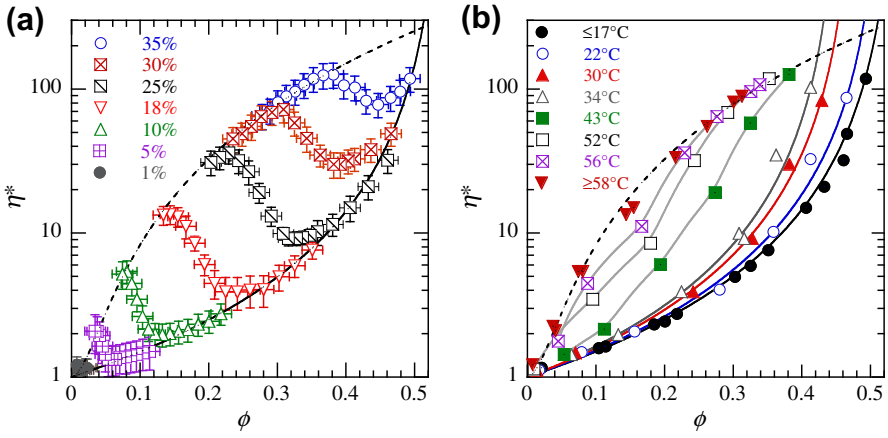

Fig. 7. (a) Reduced viscosity as a function of the hard sphere volume fraction ϕ for the different mass concentrations (semi-log scale). The solid black line corresponds to the "low viscosity" limit: $\eta^* = (1 - \phi/0.54)^{-2}$, while the dashed line corresponds to the "high viscosity" limit: $\eta^* = 1 + 2.5\phi + k_2\phi_2 + k_3\phi_3$. (b) $\eta^*(T)$ as a function of ϕ for different temperatures (semi-log scale). Solid lines correspond to the curve fits of η^* for $T \leqslant 34$ °C using: $\eta^* = (1 - \phi/\phi^*)^{-2}$, the dashed black line corresponds to the curve fit of η^* for $T = 58$ °C using: $\eta^* = 1 + 2.5\phi + k_2\phi_2 + k_3\phi_3$. Grey solid lines are guides for the eyes.

between micelles that has the upper hand and therefore the viscosity increases although the micelles volume fraction decreases. Finally, at higher temperature (for lower ϕ), the decrease in ϕ is again dominant (likely because then the effects of the micelle–micelle interaction on the hydrodynamic interactions do not change much with T) and consequently the viscosity decreases again. Nevertheless, it is difficult to go beyond a simple qualitative analysis, because the evolution of the viscosity as a function of the volume fraction for solutions of attractive spheres is unknown theoretically.

4.3. Dynamics

4.3.1. Relaxation of concentration fluctuations and sedimentation coefficient

Considering $C_{12}E_8$ solutions as an incompressible, athermal, binary fluid (the solvent and the micelles), the collective diffusion coefficient D_c results from the competition between thermodynamic effects, which tend to restore equilibrium, and the hydrodynamic drag, which slows down the micelle motion, and thus the return to equilibrium. Thereby, D_c can be expressed as a function of the volume fraction of micelle as follows [63]:

$$D_c = \frac{1}{\zeta(\phi_m)}\left[\phi_m\left(\frac{\partial \Pi}{\partial \phi_m}\right)\right] = \frac{1}{\chi_T(\phi_m)\zeta(\phi_m)} \tag{7}$$

where Π is the osmotic pressure of the solution and $\chi_T(\phi_m)$ its isothermal osmotic compressibility: $\chi_T(\phi_m)^{-1} = N_m k_B T/(VS(0,\phi_m)) = \phi k_B T/(V_{hs}S(0,\phi))$, where $S(0,\phi)$ is the structure factor of the system at $q = 0$. $\zeta(\phi_m)$ is a collective friction coefficient that accounts for the hydrodynamic drag felt by the micelles in the solution. For $q \to 0$, this term can be written as follows: $\zeta(\phi_m)^{-1} = K(\phi_m)/(N_m\zeta_0) = V_{hs}K(\phi)/(\phi\zeta_0)$, where $K(\phi)$ is the sedimentation coefficient (the hydrodynamic function in the limit $q \to 0$) and ζ_0 the friction term that acts on an isolated micelle: $\zeta_0 = 6\pi\eta_S r$, η_S being the solvent viscosity and r the micelle radius.

$$D_c = \frac{k_B T}{6\pi\eta_w r}\frac{K(\phi)}{S(0,\phi)} = D_0\frac{K(\phi)}{S(0,\phi)} \tag{8}$$

Fig. 8a displays D_c/D_0 as a function of the volume fraction of hard spheres ϕ for the different samples ($\phi(w_S, T) = w_S$ exp$(-(T-46)/73)$; $D_0 = k_B T/6\pi\eta_S r_{mic}$, where r_{mic} is taken as the average of the micelle's radius from SANS data, assuming a linear increase with T for temperatures not investigated by SANS). For each concentration, this quantity increases with ϕ. In Fig. 8b is shown the "isothermal" ratio: $D_c(T)/D_0(T)$ as a function of ϕ (*i.e.* same data as in Fig. 8a but gathering all data taken at the given temperature T). For each investigated temperature, the evolution of D_c/D_0 as a function of ϕ can be fitted to polynomial functions of degree 3: $1 - \lambda_1\phi + \lambda_2\phi^2 + \lambda_3\phi^3$, where λ_1, λ_2 and λ_3 are always positive; λ_1, λ_2 increasing with T while λ_3 decreases. The negative sign in front of λ_1 signals the existence of an attractive interaction between micelles [63–65]. (The obtained values of λ_1 are displayed as a function of T in Fig. 8c.) It is easy to show that $S(0,\phi)$ is given by the following relation (Supporting Material: Part C.2.2):

$$S(q \to 0, \phi) = \frac{(1-\phi)^4}{(1+2\phi)^2 - \phi^3(4-\phi) + \phi(1-\phi)^4(aU_{rep} + bU_{att})} \tag{9}$$

where $a = 3\delta_{rep}/(\pi R)$ and $b = 3\delta_{att}/(\pi R)$. Hence, $1/S(0,\phi)$ is always an increasing function of ϕ. Therefore, to understand the evolution of $D_c(T)/D_0(T)$ with ϕ that of the sedimentation coefficient must be figured out.

Values of K are estimated and shown in Fig. 8d. For a given mass concentration, the values of K increase with T almost linearly with a slope that seems to be independent of w_S (Fig. 8d inset). For each temperature, $K(\phi)$ decreases and can always be fitted to a polynomial function of degree 4 (Fig. 8d): $1 - \gamma_1\phi + \gamma_2\phi^2 - \gamma_3\phi^3 + \gamma_4\phi^4$, with $\gamma_1, \gamma_2, \gamma_3, \gamma_4 > 0$, which all increase with T (the obtained values of γ_1 are displayed as a function of T in Fig. 8c). There is no theoretical prediction for the sedimentation coefficient of systems with such an interaction potential; nevertheless, its behaviour can be understood easily. At low volume fraction ($\phi < 0.25$), $K(\phi) < K_{hs}(\phi)$, where $K_{hs}(\phi)$ is the sedimentation coefficient expected for a pure monodisperse hard sphere system (with a Péclet number $Pe \ll 1$): $K_{hs}(\phi) = (1-\phi)^{6.55}$ [66–70] (solid line in Fig. 8d); hence, $K(\phi)$ decreases faster than that of pure hard sphere dispersions. This is simply due to the attractive interaction between micelles that increases the population of nearby particles, which leads to a stronger hydrodynamic interaction and friction, increasing the sedimentation velocity [71,72]. Moreover, $K(\phi)$ is expected to decay all the faster with ϕ as the attraction between particles is strong. Thus, the increase in γ_1 with T (Fig. 8c) arises from the strengthening of the attraction between $C_{12}E_8$ micelles with temperature. (From there, we understand the increase in λ_1 as T rises; for low volume fractions $1/S(0,\phi)$ can be written as: $1/S(0,\phi) \approx 1 + B_2\phi + B_3\phi^2$, where B_2 and B_3 are the second and third Virial coefficients, respectively, thus: $\lambda_1 = \gamma_1 - B_2$ and B_2 decreases as the attractive interaction between micelles enhances.) On the other hand, for $\phi > 0.25$, it is observed that $K(\phi)$ is larger than $K_{hs}(\phi)$; that is, $K(\phi)$ diminishes less quickly than that of pure hard sphere dispersions. For these volume fractions, for which the separation distance between micelles becomes less than 15 Å, one can imagine the steric interaction between micelles begins to affect their motion, reducing the near-field hydrodynamic interactions, which, therefore, slows down the sedimentation velocity [73–75]. Hence, the strong increase in D_c/D_0 with ϕ for high volume fractions is the signature of the steric repulsion between $C_{12}E_8$ micelles.

For a given mass concentration, the evolution of D_c as T increases (shown in Fig. 2) is due to the competition between the decrease in volume fraction of micelles and the interaction growth that affects the hydrodynamic interactions. In Fig. 8c, we display the values of the second Virial coefficient B_2 as a function of T, values measured from SANS experiments (empty circles; Supporting Material: Part C2.4) and QELS results (full circles; there $B_2(T)$ is simply given by: $\gamma_1(T) - \lambda_1(T)$). Both values are very close to each other, which points that QELS and SANS measurements are consistent. As expected, B_2 deceases upon temperature increase, so with the attraction between micelles and this effect seems to enhance above 30 °C. Therefore, results on the relaxation of concentration fluctuations are in full agreement with SANS and viscosity results.

4.3.2. Slow relaxation

Slow relaxation was already reported in many colloidal systems [38,76,77], and there are several possible explanations for the origin of such a mode. A possible origin has been proposed by Weissman [78] and Pusey et al. [79]. In concentrated colloidal dispersions, a slight polydispersity in size, or optical index, may lead to a slow diffusive mode unaccounted-for by the usual hydrodynamic theory. Its relaxation rate is given by self-diffusion, but with the solvent viscosity η_w replaced by the low shear viscosity of the solution η_{sample}, thus: $D_{Self} = k_B T/(6\pi\eta_{sample}R_S)$. Using the measured values of η_{sample}, it is obtained that the values of R_S seems to be constant, but of the order of 130 ± 30 nm, about 45 times larger than the hydrodynamic radius of $C_{12}E_8$ micelles. We therefore discard this explanation. Another kind of slow relaxation exists in concentred solutions of colloidal spheres: it is linked to the jump of the spheres out of a "virtual cage" made up by their neighbours [80,81]. This relaxation, however, has only been observed close to the disordered–ordered phase transition, for volume fractions larger than 0.45 and is subdiffusive. As mentioned above, this slow mode is still observed for the sample with $w_S = 10$ wt.% at 50 °C,

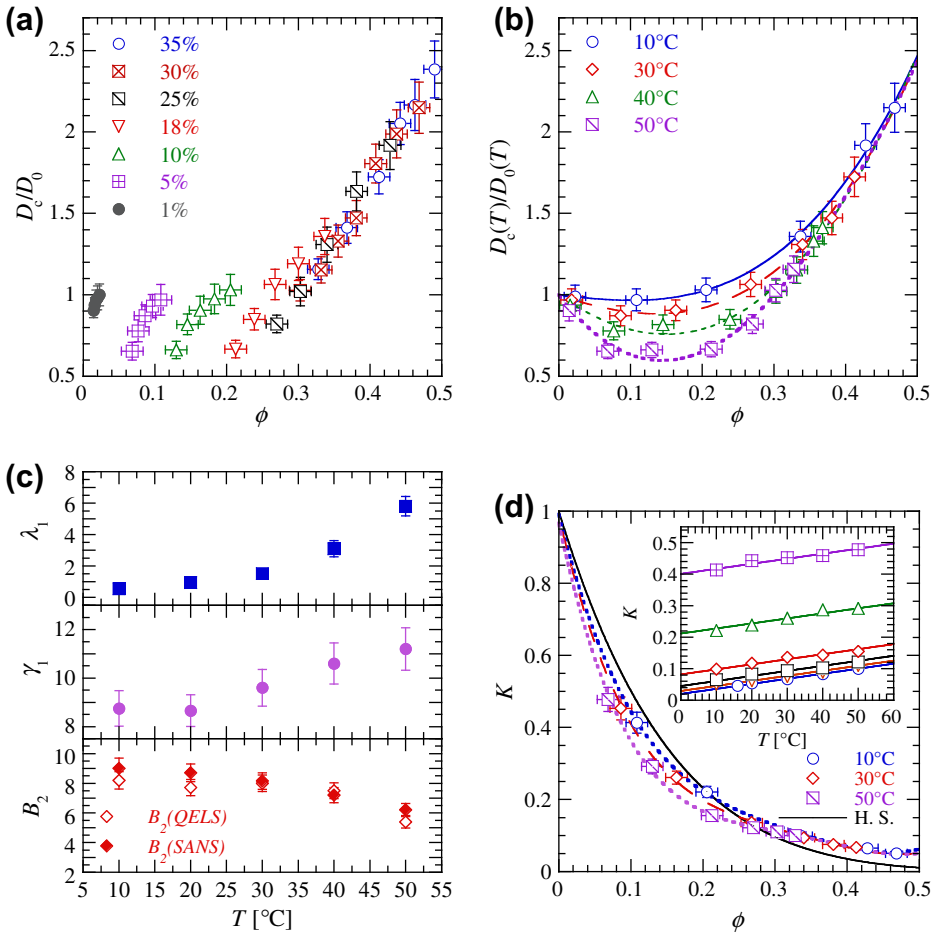

Fig. 8. (a) D_c/D_0 as a function of the volume fraction of hard spheres ϕ for the different investigated mass concentrations. (b) $D_c(T)/D_0(T)$ ratio as a function of ϕ, for: 10 °C; 30 °C; 40 °C and 50 °C, respectively. The solid and dashed lines are fits to the data using the function: $1 - \lambda_1\phi + \lambda_2\phi^2 + \lambda_3\phi^3$ (we did not display the values of $D_c(T)/D_0(T)$ at 20 °C, for clarity reasons). (c) Temperature evolutions of: λ_1, γ_1 and B_2 (the second Virial coefficient obtained from QELS and SANS data). (d) Sedimentation coefficient K as a function of the ϕ ($K(\phi) = S(0, \phi)D_c(\phi)/D_0$), for: 10 °C; 30 °C; and 50 °C (we did not display $K(\phi)$ at 20 °C and 40 °C, for clarity reasons). Dashed lines are fits to the data using the function: $1 - \gamma_1\phi + \gamma_2\phi^2 - \gamma_3\phi^3 + \gamma_4\phi^4$; the solid black line is the evolution of the sedimentation coefficient expected for a pure monodisperse hard sphere system. Inset: temperature evolution of the sedimentation coefficient for the different investigated mass concentrations (same set of markers as in Fig. 8a).

hence down to a hard sphere volume fraction ϕ of about 0.1 and is diffusive, or super-diffusive.

Here, we may compare our results with those obtained by Brown et al. [38]. They performed QELS measurements in the mass fraction range 0.5–15% and temperatures between 14 and 54 °C. For $w_S \geqslant 10$ wt.%, they also observed two relaxation modes. Our values of the diffusion coefficient are of the same order of magnitude as theirs. However, their observations on the evolution of the D_c/D_0 ratio as a function of w_S for a given temperature are slightly different from ours. Although they observe the existence and the strengthening of an attraction between $C_{12}E_8$ micelles upon temperature increase, contrary to us, they do not observe the effects of this attraction below 32 °C. For $T < 32$ °C, they find a linear increase in D_c/D_0 with w_S and thus positive λ_1. We do not understand this discrepancy. The conclusions we draw from our results are, nevertheless, qualitatively, in good agreement with their results.

4.3.3. Local order relaxation; viscoelasticity

Viscoelastic behaviour is seen for micellar solutions with hard sphere volume fractions higher than 0.3–0.35. Following Refs. [44,82], we made the assumption that this viscoelastic behaviour is due to the relaxation of the local order caused by the micelle–micelle interaction. In this framework, τ is the local order relaxation time, τ_ξ, which is given by: $\xi^2/6D_c$ [82], where D_c is the collective diffusion coefficient and ξ the correlation length of the micelle–micelle distance fluctuations that characterises the spatial range of the local order. Using the measured values of D_c and ξ (Supporting Material: Part C2.5, Fig. S.13), the values of τ_ξ can be estimated. They are shown in Fig. 9a together with the measured Maxwell relaxation times τ.

One observes that values of τ_ξ and τ are of the same order of magnitude and both decrease with T in similar ways. In Fig. 9b, the measured values of τ are plotted as a function of ϕ; τ increases with ϕ. According to the model of the local order relaxation, τ is expected to diverge with ϕ as ξ^2, that is, as: $(1 - \phi/0.54)^{-1.5}$, which seems to be the case for both samples. As D_c is larger for $w_S = 35$ wt.% than for $w_S = 30$ wt.%, for a given ϕ, τ is expected to be longer for the less concentrated sample. That is what observed (Fig. 9b). These set of results strongly support our hypothesis on the origin of the viscoelasticity of these mixtures and therefore we believe that this behaviour is due to the relaxation of the local structure of micellar solutions.

Using what we learned about this system, it is easy to understand the behaviour of G_∞ with T (Fig. 3c). When T is increased from very low temperatures, the decrease in the effective volume fraction of micelles, which should cause a decrease in G_∞, and the increase in the direct interaction between micelles, which opposes the relative motion of micelles resulting in an increase in G_∞, compensates each other. Thus, at first, G_∞ remains almost constant. Then, it is the increase in the interaction between micelles

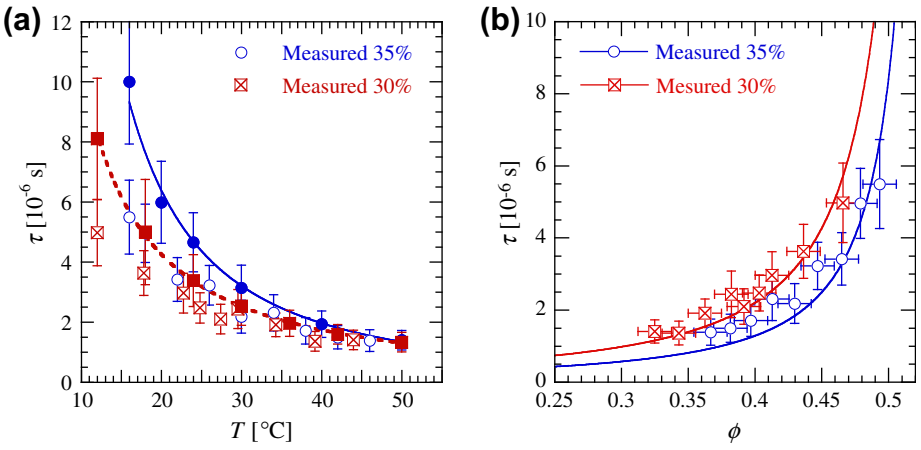

Fig. 9. (a) Evolution as a function of T of the measured values of τ for samples with w_S = 35 and 30 wt.% and estimated values of τ_ξ using SANS and QELS results; w_S = 35 wt.%: full circles-solid line, w_S = 30 wt.%: full square-dashed line (in semi-log scale). (b) Measured values of τ as a function of the hard sphere volume fraction ϕ, the solid lines are fits of these data to: $A\ (1-\phi/0.54)^{-1.5}$.

that takes over and G_∞ increases although the micelle volume fraction keeps decreasing.

It should be noted that the rheological behaviour of $C_{12}E_8/H_2O$ mixtures is very different from that exhibited by wormlike micelle solutions consisting of non-ionic surfactants such as, for example, $C_{12}E_5$ and $C_{12}E_6$ [44,45,82] or of ionic surfactants [83] that display viscoelastic properties at much lower concentrations, and with much slower relaxation times. Furthermore, $C_{12}E_5$ ([45] and Supporting Material: Part C.3, Fig. S.14) and $C_{12}E_6$ [44] solutions have a more complex behaviour with two Maxwell relaxation processes in the accessible frequency range.

5. Summary and conclusions

The aim of this work was to provide information on the structure, thermodynamics and dynamics of the isotropic phase of spherical non-ionic surfactant micelles. For such a purpose, we investigated $C_{12}EO_8$/water mixtures over a wide range of concentrations and temperatures (*i.e.* 1–35 wt.% in mass fraction and 10–60 °C in temperature). Our approach, crossing several experimental techniques: Small-Angle Neutron Scattering (SANS), Quasi Elastic Light Scattering (QELS) and High Frequency Rheology proved useful for a complete understanding of this system properties. Our results show that the temperature behaviours of the structural, thermodynamic, dynamic and rheological properties of these solutions are fully monitored by the temperature-induced changes in the hydration of octa-ethylene–glycol chains. These changes in the hydration of E_8 chains control both the pair interaction potential and the volume fraction of micelles. Therefore, the temperature evolutions of the physical properties can be fully explained by the temperature-induced competition between variations in the volume fraction of micelles and interactions. Even if this was suspected, it had never been demonstrated clearly before. The main results that our investigation demonstrates and we wanted to bring out in this article are the following.

- $C_{12}E_8$ molecules in water associate to form spherical micelles, and the size of which is constant with concentration and increases slightly with T (at least up to about 60 °C). According to the $C_{12}E_8/H_2O$ phase diagram, it is likely that this does not hold any longer at higher concentrations (at about 40 wt.%, close to L1/H1 transition) or higher temperatures (close to the critical consolute temperature; above 70 °C). This is in total agreement with previous results [25,29–32], but completely at odds with the results of Hedin et al. [33]. We believe that Hedin et al. misinterpreted their data; indeed, they investigated only one sample with w_S = 5 wt.% and consider no interaction between $C_{12}E_8$ micelles, which is a highly questionable assumption.
- For a given concentration of $C_{12}E_8$, because of the temperature-induced changes in E_8 chain hydration, the number of micelles in solution is not constant with temperature. The volume fraction increases as T decreases: $\phi(w_S, T) = A w_S \exp(E/k_BT)$, with $E = (1.73 \pm 0.15) \times 10^{-20}$ J (*i.e.* $E = (4.2 \pm 0.4) k_BT$) and $A = 0.0186 \pm 0.0005$. This explains why an isotropic–ordered phase transition is observed in this system upon decreasing T in the concentration range 31–38 wt.%. In this range, it exists a temperature greater than 0 °C below which the effective volume fraction of hard spheres exceeds the value at which hard sphere solutions undergo a disordered–ordered phase transition.
- The interaction potential between $C_{12}E_8$ micelles is more complicated than previously described [25,34]. SANS, QELS, as well as rheology measurements demonstrate that the micelle–micelle interaction is temperature dependant and can be described as the superposition of three contributions: a hard core, with a range shorter than the micelle radius, an additional repulsive potential and an attractive potential. The strength of the attractive part increases with T, very likely due to the change in the solvent quality for the ethylene oxide chains as temperature rises (water turning from good to bad). The additional repulsive potential is of steric origin, due to the interpenetration of the surfactant hydrophilic heads, and to our knowledge, this additional repulsion has never been described before. This repulsion seems to monitor the physical properties of concentrated solutions (typically for ϕ larger than about 0.25), well before the concentration at which E_8 chains start to overlap ($\phi > 0.39$).
- Our investigation provides new information on the dynamics of these mixtures that reflect the complexity of the interaction potential between the $C_{12}E_8$ micelles. It reveals that concentrated solutions exhibit a viscoelastic behaviour that can be described by a simple Maxwell model, with a relaxation time below 10^{-5} s. This viscoelastic behaviour originates in the relaxation of the local order due the micelle–micelle interaction. To our knowledge, there is so far only one study on the viscoelastic properties of these systems [44]. Nevertheless, some points of the dynamics of these systems still remain unclear. In QELS

experiments, we observe a puzzling slow relaxation mode, the origin of which could not be found out; we can, however, rule out the size polydispersity of micelles as well as cage rearrangement as causes.

We believe that our conclusions may also apply to other C_iE_j–water mixtures as well as to pluronic–water mixtures, since in all these systems temperature-induced dehydration of the head groups must modify both the aggregation number and the interaction potential. It is highly likely that C_iE_j molecules having an E_j group much bigger than their alkyl chain (*e.g.* $C_{12}E_j$, with $j \geqslant 9$) form spherical micelles in water and the structure, thermodynamics and dynamics of their isotropic phases should exhibit similar concentration and temperature behaviours as those of $C_{12}E_8$ micellar solutions. Our results should be applicable to dispersions of spherical colloids coated with PEO or PEG chains, which should have the same kind of temperature dependence of the interaction potential between particles. Because the interaction between micelles is easily tuneable by means of temperature, one can imagine that these systems could be used as model systems for investigating the physics of spherical colloids with weak interactions.

Acknowledgments

The authors would like to express their thanks to: Dr B. Farago for helping them with the SANS experiments at the Institut Laue-Langevin (ILL) in Grenoble, France; Professor P. Pusey and Professor U. Olson for answering their questions; Professor T. Biben, Professor P. Panizza, Professor F. Nallet and Dr V. Vidal for helpful and fruitful discussions.

Appendix A. Supplementary material

Supplementary data associated with this article can be found, in the online version, at http://dx.doi.org/10.1016/j.jcis.2012.10.039.

References

[1] J.R. Brotherus, L. Jacobsen, P.L. Jorgensen, Biochim. Biophys. Acta 731 (1983) 290.
[2] M. Le maire, S. Kwee, J.P. Andersen, J.V. Moller, Eur. J. Biochem. 129 (1983) 525.
[3] J.R. Casey, R.A.F. Reithmeier, J. Biol. Chem. 266 (1991) 15726.
[4] J.V. Moller, M. Le maire, J. Biol. Chem. 268 (1995) 18659.
[5] D. Otten, L. Löbbecke, K. Beyer, Biophys. J. 68 (1995) 584.
[6] M.R. Wenk, T. Alt, A. Seelig, J. Seelig, Biophys. J. 72 (1997) 1719.
[7] U. Kragh-Hansen, M. le Maire, J.V. Moller, Biophys. J. 75 (1998) 2932.
[8] M. Vasilescu, D. Angelescu, M. Almgren, A. Valstar, Langmuir 15 (1999) 2635.
[9] X. Li-Blatter, P. Nervi, A. Seelig, Biochim. Biophys. Acta-Biomembranes 1788 (2009) 2335.
[10] C.C. Domingues, A. Ciana, A. Buttafava, B.R. Casadei, C. Balduini, E. de Paula, G. Minetti, J. Membrane Biol. 234 (2010) 195.
[11] C. Montigny, B. Arnou, P. Champeil, Biochem. Biophys. Res. Commun. 391 (2010) 1067.
[12] K. Shinoda, J. Colloid Interface Sci. 34 (1970) 278.
[13] F. Harusawa, S. Nakamura, T. Mitsui, Colloid Polym. Sci. 252 (1974) 613.
[14] A.A. Ali, B.A.J. Mulley, Pharm. Pharmacol. 30 (1978) 205.
[15] J.C. Lang, R.D.J. Morgan, Chem. Phys. 73 (1980) 5849.
[16] G.J.T. Tiddy, Phys. Rep. 57 (1980) 1.
[17] P.G. Nilsson, B. Lindman, J. Phys. Chem. 87 (1983) 4756.
[18] D.J. Mitchell, G.J.T. Tiddy, L. Waring, T. Bostock, M.P.J. McDonald, Chem. Soc. Faraday Trans. I (79) (1983) 975.
[19] C.D. Adam, J.A. Durrant, M.R. Lowry, G.J.T. Tiddy, J. Chem. Soc. Faraday Trans. I (80) (1984) 789.
[20] B. Andersson, G. Olofsson, Colloid Polym. Sci. 265 (1987) 318.
[21] J. Sjöblom, P. Stenius, I. Danielsson, in: M.J. Schick (Ed.), Nonionic Surfactants, Marcel Dekker, New York, 1987, p. 369.
[22] R.G. Laughlin, in: The Aqueous Phase Behavior of Surfactants, Academic Press, London, 1994.
[23] B. Medhage, M. Almgren, J. Alsins, J. Phys. Chem. 97 (1993) 7753.
[24] M. Corti, V. Degiorgio, J.B. Hayter, M. Zulauf, Chem. Phys. Lett. 109 (1984) 579.
[25] M. Zulauf, K. Weckström, J.B. Hayter, V. Degiorgio, M. Corti, J. Phys. Chem. 89 (1985) 3411.
[26] L. Cantù, M. Corti, C. Minero, R. Piaza, V. Degiorgio, J. Colloid Interface Sci. 105 (1985) 628.
[27] L. Cantù, M. Corti, V. Degiorgio, H. Hoffmann, W. Ulbricht, J. Colloid Interface Sci. 116 (1987) 384.
[28] G. Dietler, D.S. Cannell, Phys. Rev. Lett. 60 (1988) 1852.
[29] T. Matsumoto, H. Zenkoh, Colloid. Polym. Sci. 268 (1990) 536.
[30] B. Lindman, H. Wennerström, J. Phys. Chem. 95 (1991) 6053.
[31] M. Jonstromer, B. Jonsson, B. Lindman, J. Phys. Chem. 95 (1991) 3293.
[32] D. Danino, Y. Talmon, R. Zana, J. Colloid Interface Sci. 186 (1997) 170.
[33] N. Hedin, T.Y. Yu, I. Furó, Langmuir 16 (2000) 7548.
[34] M. Imai, I. Yoshida, T. Iwaki, K. Nakaya, J. Chem. Phys. 122 (2005) 044906.
[35] G. D'Arrigo, G. Briganti, M. Maccarini, J. Phys. Chem. B 110 (2006) 4612.
[36] X.B. Zeng, Y.S. Liu, M. Impéror-Clerc, J. Phys. Chem. B 111 (2007) 5174.
[37] A. Gonzalez-Perez, U. Olsson, Soft Matter 4 (2008) 1625.
[38] W. Brown, Z. Pu, R.J. Rymden, Phys. Chem. 92 (1988) 6086.
[39] T. Kato, S. Anzai, T. Seimiya, J. Phys. Chem. 94 (1990) 7255.
[40] H. Ruf, Langmuir 18 (2002) 3804.
[41] P. Lindner, J. Appl. Cryst. 33 (2000) 807.
[42] S.R. Kline, J. Appl. Cryst. 39 (2006) 895.
[43] M. Cagnon, G. Durand, Phys. Rev. Lett. 45 (1980) 1418.
[44] D. Constantin, Langmuir 19 (2003) 2554.
[45] Unpublished Data.
[46] J.D. Ferry, in: Viscoelastic Properties of Polymers, John Wiley & Sons, New York, 1980.
[47] A.J. Archer, D. Pini, R. Evans, L. Reatto, J. Chem. Phys. 126 (2007) 014104.
[48] J.-P. Hansen, I.R. McDonald, in: Theory of Simple Liquid, second ed., Academic Press, London, 1991.
[49] M.S. Wertheim, Phys. Rev. Lett. 10 (1963) 321.
[50] E.J. Thiele, Chem. Phys. 39 (1963) 474.
[51] P.N. Pusey, W. van Megen, Nature 320 (1986) 340.
[52] V.J. Anderson, H.N.W. Lekkerkerker, Nature 416 (2002) 811.
[53] E. Freyssingeas, F. Nallet, D. Roux, Langmuir 12 (1996) 6028.
[54] V. S Marinov, Z.S. Nickolov, H. Matsuura, J. Phys. Chem. B 105 (2001) 9953.
[55] S. Schrödle, G. Hefter, W. Kunz, R. Buchner, Langmuir 22 (2006) 924.
[56] E. Freyssingeas, A. Martin, D. Roux, Eur. Phys. J. E 18 (2005) 219.
[57] J.N. Israelachvili, S. Marcelja, R.G.Q. Horn, Rev. Biophys. 13 (1980) 121.
[58] J. N. Israelachvili, Intermolecular and Surface Forces; Steric and Fluctuation Forces, second ed., Academic Press, London, 1991 (Chapter 14).
[59] D. Quemada, Rheol. Acta 16 (1977) 82.
[60] C. Allain, M. Cloitre, J. Chem. Phys. 100 (1994) 4537.
[61] V. Trappe, V. Prasad, L. Cipelletti, P.N. Segrè, D.A. Weitz, Nature 411 (2001) 772.
[62] M. Sztucki, T. Narayanan, G. Belina, A. Moussaid, F. Pignon, H. Hoekstra, Phys. Rev. E 74 (2006). Art. No.: 051504.
[63] P.N. Pusey, R.J.A. Tough, Particles interactions, in: R. Pecora (Ed.), Dynamic Light Scatterring: Application of Photons Correlation Spectroscopy, Plenum Press, New York, 1985 (Chapter 4).
[64] B.U.J. Felderhof, Phys. A 11 (1978) 929.
[65] R. Tuinier, E. ten Grotenhuis, C. Holt, P.A. Timmins, C.G. de Kruif, Phys. Rev. E 60 (1999) 848.
[66] J.F. Richardson, W.N. Zaki, Trans. Inst. Chem. Eng. 32 (1954) 35.
[67] R. Buscall, L.R.J. White, Chem. Soc. Faraday Trans. I (83) (1987) 873.
[68] J.F. Brady, L.J. Durlofsky, Phys. Fluids 31 (1988) 717.
[69] R. Buscall, J.W. Goodwin, R.H. Ottewill, T.F. Tadros, J. Colloid Interface Sci. 85 (1982) 78.
[70] M.A. Al-Naafa, M.S. Selim, AIChE 38 (1992) 1618.
[71] P.N. Segrè, S.P. Meeker, P.N. Pusey, W.C.K. Poon, Phys. Rev. Lett. 75 (1995) 958.
[72] P.N. Segrè, P.N. Pusey, Phys. Rev. Lett. 77 (1996) 771.
[73] G.K. Batchelor, J. Fluid Mech. 52 (1972) 245.
[74] G.K. Batchelor, C.S. Wen, J. Fluid Mech. 124 (1982) 495.
[75] J.Z. Xue, E. Herbolzheimer, M.A. Rutgers, W.B. Russel, P.M. Chaikin, Phys. Rev. Lett. 69 (1992) 1715.
[76] A. Shukla, H. Graener, R.H.H. Neubert, Langmuir 20 (2004) 8526.
[77] Y. Hattori, H. Ushiki, L. Courbin, P. Panizza, Phys. Rev. E 75 (2007) 021504.
[78] M.B. Weissman, J. Chem. Phys. 72 (1980) 231.
[79] P.N. Pusey, H.M. Fijnaut, A. Vrij, J. Chem. Phys. 77 (1982) 4270.
[80] R. Sigel, S. Pispas, D. Vlassopoulos, N. Hadjichristidis, G. Fytas, Phys. Rev. Lett. 83 (1999) 4666.
[81] E.R. Weeks, D.A. Weitz, Chem. Phys. 284 (2002) 361.
[82] D. Constantin, J.-F. Palierne, E. Freyssingeas, P. Oswald, Europhys. Lett. 58 (2002) 236.
[83] J. Haldar, V.K. Aswal, P.S. Goyal, S. Bhattacharya, Ang. Chem. Int. Ed. 40 (2001) 1228.